

Constraining Dark matter annihilation with Dark Energy Survey Y3 LSBG sample

Daiki Hashimoto*

*Division of particle and astrophysical sciences, Graduate School of Science,
Nagoya University, Furocho Chikusa, Nagoya, 464-8602, Aichi, Japan*

Atsushi J. Nishizawa

*Institute for Advanced Research, Nagoya University,
Furocho Chikusa, Nagoya, 464-8602, Aichi, Japan
Division of particle and astrophysical sciences, Graduate School of Science,
Nagoya University, Furocho Chikusa, Nagoya, 464-8602, Aichi, Japan*

Masahiro Takada

*Kavli Institute for the Physics and Mathematics of the Universe (WPI),
The University of Tokyo Institutes for Advanced Study (UTIAS),
The University of Tokyo, 5-1-5 Kashiwanoha, Kashiwa-shi, Chiba, 277-8583, Japan*

(Dated: February 4, 2022)

To reveal natures of the dark matter (DM) particles, a γ -ray signal produced in annihilation processes of DM into the standard model particles has been one of the major probes. The cross-correlation between highly DM dominated structures, such as local dwarf galaxies, and observed photons in the direction of the structures, has been explored and provided stringent constraints on the annihilation rate. In our previous work, we have shown that it is sufficient to know the distance distribution of the galaxy sample and individual distance measurement is not required for constraining the annihilation rate. In this work, we apply the method to low-surface brightness galaxies (LSBGs) with unknown individual redshifts provided from the Dark Energy Survey (DES) Year 3 data. With all DES-LSBGs of $\sim 24,000$ objects, we find that the upper limits of the cross section $\langle\sigma v\rangle$ for $b\bar{b}$ channel with 95% C.L. is $\sim 3 \times 10^{-25}$ cm³/s at DM mass of 100 GeV. To be more conservative, we remove ~ 7000 LSBGs within 1° from resolved γ -ray point sources and then the constraint becomes $\sim 30\%$ weaker than the one with all samples in all DM mass ranges.

I. INTRODUCTION

As one of the most promising dark matter (DM) candidates, weakly interacting massive particles (WIMPs) [1], which are considered to be produced in the early Universe in the thermal equilibrium with the standard-model (SM) particles, have been searched in several decades. Great efforts have been kept to search for signals originated from interactions of WIMPs with SM particles [2, 3]. In the context of the astrophysics, researchers have focused on indirect searches for DM annihilation signals, particularly, emission of γ rays, positrons and neutrinos produced by the annihilation of DM particles and secondary cascade processes [e.g., 4, 5]. In terms of the γ -ray signal, the cross correlation of observed γ -ray photons with any astronomical structure, such as local galaxies, galaxy groups, clusters, the Milky Way dwarf spheroidals (MW dSphs) and the Galactic center, has been studied in numerous works [e.g., 6–13], and then upper limits on the annihilation cross-section has been provided. The most robust and stringent constraint is provided by the cross-correlation analysis using 27 MW dSphs with unresolved γ -ray background (UGRB), which is a residual photon-flux field produced by subtraction of the Galactic and isotropic emissions as well as resolved γ -ray point-source

emissions from the photon data of the *Fermi* Large Area Telescope (LAT) observation, and the upper limit with 95% C.L. is found at $\langle\sigma v\rangle \sim 2 \times 10^{-26}$ [cm³/s] at DM mass of 100 GeV [14].

In our previous work [15], low-surface brightness galaxies (LSBGs) have been proposed as target objects to probe the γ -ray signal (LSBGs have been used for the probe in a few works, such as Ref. [16]). LSBG has several favorable aspects for the purpose such as being relative massive [17], highly DM-dominated [18] and expected to be quiescent in γ rays due to relatively quiescent star-forming activities [19]. We have explored the annihilation γ -ray signal in the UGRB sky performing the joint likelihood analysis with known-redshift LSBGs, which is included in a tiny fraction of a LSBG catalog produced from the Hyper Suprime-Cam (HSC) data [20]. In our another previous work [21], we have presented the method for the signal probe using all LSBGs (~ 800 objects) of the HSC-LSBG catalog. In the method, we randomly assign object redshifts from the redshift distribution of the overall sample dN/dz , which is obtained by the so-called clustering redshift method, in which we measure angular cross-correlations of LSBGs and a spectroscopic redshift (spec- z) sample as a reference sample in different redshift bins, and convert the correlations to the dN/dz amplitudes. With the joint likelihood analysis using the full sample, we have shown that it is sufficient for the DM cross-section constraint to use dN/dz of the overall catalog without measuring their individual red-

* hashimoto.daiki@f.mbox.nagoya-u.ac.jp

shifts. Moreover, we have found that the upper limit on the cross section scales with an inverse of the number of objects N , rather than \sqrt{N} .

In this work, we apply our method to the Dark Energy Survey (DES) LSBGs [22] including $\sim 24,000$ objects in the sky coverage of ~ 5000 deg². As a difference between procedures in this work and the previous work using the full HSC-LSBG sample, we consider the cross-covariance matrix of the angular cross-correlation between different redshift bins. Moreover, because variability of flux-model parameters of bright sources nearby LSBGs can significantly change the putative flux of LSBGs, we consider a better UGRB-field production for the careful estimation of the putative flux.

This paper is organized as follows. We describe datasets in our analysis in Section II, and the method for production of the UGRB field and estimate of a likelihood profile of the putative flux at LSBG position in Section III. In Section IV, we revisit the methodology of our analysis for the dN/dz measurement and composite likelihood and find the results in the composite analysis using the full sample of DES LSBGs in Section V. Finally, we summarize our study in Section VI.

II. DATASET

A. LSBG sample

DES is an imaging survey of five optical broad bands (g, r, i, z and Y) covering ~ 5000 deg² of the southern hemisphere using the Dark Energy Camera (DECam) [23] on the 4-m Blanco Telescope at the Cerro Tololo Inter-American Observatory. The DECam composed by 74 CCDs with a central pixel scale of $0.263''$ has a wide field of view of 3 deg². The single epoch processing pipeline `Final Cut` [24] provides reduced images and also performs source detection and measurement of galaxies with `SourceExtractor` [25], which can discover faint objects. In the Wide Survey of DES Year 3, the median coadd magnitude limits in the g, r, i, z and Y band with signal-to-noise ratio (S/N) of 10 are 24.3, 24.0, 23.3, 22.6 and 21.4, respectively [26]. For detection of LSBGs, dedicated background estimation is indispensable [24, 26].

The LSBG sample¹ [22] is constructed from the DES Y3 Gold sample as follows.

1) *Extraction of candidates from Y3 Gold catalog*

From the DES Y3 Gold coadd catalog (v2.2) [26], point-like objects are removed based on the size, surface bright-

ness, ellipticity and color cuts as

$$\begin{aligned} -0.1 < g - i < 1.4 \\ g - r > 0.7 \times (g - i) - 0.4 \\ g - r < 0.7 \times (g - i) + 0.4. \end{aligned}$$

The initial catalog after source selections above contains 419,895 candidates after this source selection.

2) *Sample selection by machine learning algorithm*

A machine learning method is used to further remove the contamination such as giant elliptical galaxies, compact objects with the diffuse foreground or background and knots of large spiral galaxies. The training set is constructed by visual inspection of the image and 7760 objects are labeled. Out of that, 640 objects are labeled as LSBGs. The machine learning classification identified 44,979 objects as the LSBG candidate. Note that the $\sim 9\%$ LSBGs are not detected with this method.

3) *Visual inspection & Sérsic model fitting*

The candidates have been visually inspected using the cutouts of $30'' \times 30''$ centered at the candidate position of each of the candidates. Finally, the light profile is fitted to the Sérsic profile to distinguish the LSBGs from other objects. All the LSBGs should pass the selections of effective radii $R_{\text{eff}}(g) > 2.5''$ and $\bar{\mu}_{\text{eff}}(g) > 24.2$ mag/arcsec².

The final catalog contains 23,790 LSBGs with the surface brightness fainter than 24.2 mag/arcsec². They are divided into 7,805 red ($g - i \geq 0.6$) and 15,985 blue ($g - i < 0.6$) LSBGs. While the red LSBGs are strongly clustering, the blue LSBGs are rather uniformly distributed. According to the stellar population model of [27], typical ages of red and blue LSBGs are 4 Gyr and 1 Gyr with $[\text{Fe}/\text{H}] = -0.4$, respectively.

B. Spec- z sample

To measure the dN/dz of the DES LSBG catalog based on the clustering redshift method, we use the final data release (DR3) of 6-degree Field Galaxy Survey (6dFGS) spectroscopic redshift sample² [28, 29], which fully overlapped with the DES sky coverage and expected redshift range. The limiting magnitudes in K, H and J band are 12.65, 12.95 and 13.75, respectively, and the catalog consists of 1,447 fields (5.7° field of view) of the telescope. In each field, 150 spectra are obtained simultaneously by individual fibers which have $100 \mu\text{m}$ ($\sim 6.7''$)-fiber diameter size of each. Due to the fiber collision, spectra of neighboring objects closer than $5'.7$ cannot be measured simultaneously.

¹ http://desdr-server.ncsa.illinois.edu/despublic/other_files/y3-lsbg/

² <http://www-wfau.roe.ac.uk/6dFGS/download.html>

In our analysis, we consider the 6dFGS sample in the DES Y1 Gold footprint [30] for the dN/dz measurement and the redshift range of the sample is limited to $z \leq 0.15$. This range would include redshifts of our LSBGs because H α -selected LSBG samples reside within a few hundreds Mpc [19, 31]. As described in the DR3 report [29], we only use samples with the redshift-quality flag $Q = 3, 4$.

C. LAT photon data

To probe γ -ray signal from the DM annihilation, we explore the γ -ray data by *Fermi*-LAT collected from Oct. 27, 2008 to July 6, 2021 and take the photon event class P8R3 SOURCE and the instrument response function for the event class P8R3 SOURCE V3 as the photon count data for analyzing point sources recommended by the Fermi collaboration [32]. We select the photons satisfying the criteria of `DATAQUAL>0 & LATCONFIG==1`. In our work, we select sky regions including the survey footprint of the DES Y3, which are composed by 43 regions of interest (ROIs). Every ROI is a patch of $20^\circ \times 20^\circ$ square region with 0.1° spatial grid size allowing 2.5 deg overlaps with the adjoining ROIs. In order to define the photon energy range to be used in our analysis, we need to consider the two distinct effects: in lower energy ranges, photons around bright sources likely leak to the neighboring pixels due to broadening of the LAT point-spread function (PSF) while in higher energy ranges, the photon statistics decreases. Therefore, we limit the range of photon from 500 MeV to 500 GeV and within that range, the photon energy is further binned in logarithmically equally spanned in 24. To avoid a contamination of photons produced by interactions of cosmic rays with the Earth's atmosphere, we exclude the photon data of zenith angles larger than 100° . In the LAT data analysis, we use the open-source package `fermipy(v1.0.1)` [33], which is based on the `Fermi Science Tools(v2.0.8)` [34].

III. UGRB FLUX AT THE LSBG POSITION

A. UGRB construction

Before analyses for probing the DM annihilation signal, we construct the UGRB sky from the observed photon data, which needs to estimate contributions from bright γ -ray sources to the total emission in our ROIs. The bright sources are three types of sources; the diffuse emission of Galactic and isotropic component as well as resolved point sources by the LAT. For modeling fluxes of these sources, we adopt the standard Galactic (`gll_iem.v07.fits`) and isotropic template

(`iso_P8R3_SOURCE_V2.v01.txt`)³ for the Galactic and isotropic diffuse emission model, respectively. We derive model fluxes of resolved γ -ray sources from the 4FGL-DR2 catalog⁴ [35, 36].

First of all, for the UGRB construction, we perform the maximum likelihood analysis in each ROI to fit spectral parameters for all the diffuse and cataloged models above to the photon data. As described in Ref. [36], the catalog contains point sources with test statistics (TS) above a detection threshold ($TS \geq 25$) in the 4FGL catalog but below in 4FGL-DR2. In our likelihood run, we exclude flux models of those cataloged sources. In addition, we perform procedures for the point-source detection in our ROIs. The photon statistics in our analysis is larger than that in the 4FGL-DR2 catalog, because the observation-time interval in our data is $\sim 20\%$ longer than one in the 4FGL-DR2 catalog. Therefore, there should be new point sources of $TS \geq 25$ in our ROIs. To detect source candidates, we run the `find_sources` method in the `fermipy` pipeline, applying a flux model of a point-like test source with a power-law spectrum with an amplitude parameter α . To quantify the significance of excess of the candidate flux in the UGRB we constructed in the likelihood run above, we define a TS value as follows [37, 38],

$$TS \equiv 2\Delta \log \mathcal{L}_{\max},$$

where $\Delta \log \mathcal{L} \equiv \log \mathcal{L}(\mathcal{D}, \theta|\alpha) - \log \mathcal{L}(\mathcal{D}, \theta|\alpha = 0)$. (1)

\mathcal{D} is the observed photon count. θ is the best-fit model parameters of the diffuse emission models as well as resolved sources in the 4FGL-DR2 catalog with $TS \geq 25$. $\Delta \log \mathcal{L}_{\max}$ denotes the maximum delta-likelihood when varying the candidate's flux amplitude α . As a result, we find 79 new point sources in ROIs ($\sim 11\%$ of all resolved sources) excluding duplicates in overlapping areas with neighboring ROIs. After identifying positions of new sources with $TS \geq 25$, we fit their spectral amplitudes and indexes to the UGRB-photon flux.

In Figure 1, we show some samples of observed-photon and UGRB maps for different two ROIs, accumulated over all energy bins. The cross and plus markers represent point sources in the 4FGL-DR2 catalog with $TS \geq 25$ and new ones we found, respectively.

B. Flux likelihood profile

In this section, we describe a method to estimate the putative γ -ray flux at the LSBG position in the UGRB field. For the flux determination of faint sources with TS values of less than 1, the Fermi collaboration has recommended the Bayesian method [39]. Accordingly, we

³ <https://fermi.gsfc.nasa.gov/ssc/data/access/lat/BackgroundModels.html>

⁴ <https://heasarc.gsfc.nasa.gov/W3Browse/fermi/fermilpsc.html>

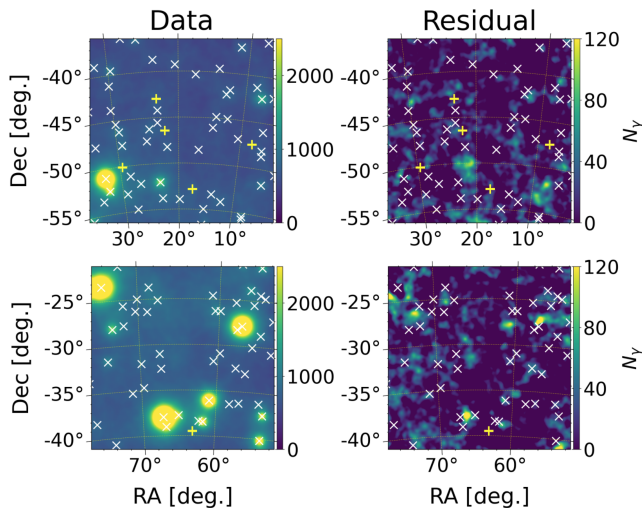


FIG. 1. Samples of the photon-count data in two different ROIs (left panels) and corresponding UGRB maps (right panels) in the energy range of $500 \text{ MeV} < E_\gamma < 500 \text{ GeV}$. The cross markers and plus signs represent positions for the 4FGL point sources and for new ones we find, respectively. The color scale represents photon counts.

estimate the UGRB flux likelihood profile at the LSBG position assuming a power-law flux model with an amplitude parameter α , using the delta-likelihood definition in Equation 1.

As mentioned in a relevant work for the UGRB-flux estimation at a faint source position [8], the putative fluxes of LSBGs can be largely affected by the variability of model parameters of bright sources in ROIs as well as neighboring resolved sources. Therefore, we revisit the UGRB construction around the LSBG position to perform a recalibration for the model parameters in the following steps. First, for sources with $TS > 1000$ in our ROIs, we free all the model parameters. Also, for all resolved sources within 3° from the LSBG position, we free all the model parameters for $400 < TS \leq 1000$ and only the amplitude parameter for $25 \leq TS \leq 400$. Then, all the freeing parameters are fit to the observed photon data by the `fit` method in `Fermipy`. Note that model parameters except for freed ones are fixed to the values in the UGRB in Section III A. After all model parameters fixed, we add the LSBG flux model as a simple power-law model with an amplitude parameter α in the UGRB field and obtain the flux likelihood profile by varying α . We find that TS values of the LSBG flux models are lower than 1 in most energy bins.

IV. METHODOLOGY

In this section, we revisit methodology for the cross-section constraint with a large number of objects without individual redshift. The method follows our previ-

ous work [21] but we introduce the cross covariance between different redshift bins in the dN/dz measurement for more realistic sampling of the redshift distribution.

A. dN/dz measurement of DES-LSBGs

We measure the redshift distribution of the DES-LSBG sample using the cross-correlation method with the spec- z sample in the same sky. To extract the clustering information, we measure the angular cross-correlation function between the LSBG sample and the 6dFGS spec- z sample as the spec- z sample. Assuming the linear galaxy bias, we can measure the redshift distribution, dN_L/dz . For measurement of the cross correlation, we use the Landy-Szalay estimator [40] with 20 logarithmic angular bins in the range of $0.1 < \theta < 5.0$ [deg], using an open software package `treecorr` (v4.2.3) [41]. Note that we ignore the redshift evolution of the biases within each redshift bin because the redshift range $0 < z < 0.15$ is narrow. We also assume that the evolution of DM clustering within the range is simply scaled with linear-growth factor.

The statistical uncertainty on the measured dN/dz is evaluated with the 100 jackknife subsamples ($\sim 50 \text{ deg}^2$ for each). The full covariance matrix of the projected correlation function can be expressed as

$$C_{ij}^{\alpha\beta} = \frac{N_{\text{JK}} - 1}{N_{\text{JK}}} \sum_{k=1}^{N_{\text{JK}}} [w_{ik}^\alpha - \hat{w}_i^\alpha][w_{jk}^\beta - \hat{w}_j^\beta], \quad (2)$$

where w_{ik}^α is the measured correlation function in the α -th redshift and i -th angular bin measured on the k -th jackknife subsample. \hat{w}_i^α is the average of w_{ik}^α over all jackknife subsamples ($N_{\text{JK}}=100$). The dN/dz is measured by integrating the correlation function across the angular scales with appropriate weight, here $w = \theta^{-1}$ [42], the covariance can be therefore,

$$\bar{C}^{\alpha\beta} = \sum_{ij} C_{ij}^{\alpha\beta} \theta_i^{-1} \theta_j^{-1}. \quad (3)$$

We consider that the number of galaxies in each redshift bin is parametrized as free parameters, Θ , obeying multivariate Gaussian distribution with the covariance given in the above equation. To prohibit negative amplitudes of dN/dz , we require the step-wise prior, $P(\Theta) = 0$ for $\Theta < 0$ and $P(\Theta) = 1$ otherwise. We finally apply the linear interpolation of the posterior distribution between each redshift bin and draw random values for every galaxy's redshift from the interpolated posterior distribution. To be conservative, we set the minimum distance to the objects being 25 Mpc, which is the nearest LSBG found in the HSC-LSBG sample in our previous analysis [15]. In Figure 2, we show the dN/dz for the red and blue LSBG sample with $1-\sigma$ errorbars evaluated by the error propagation from the jackknife error in the measured angular correlation.

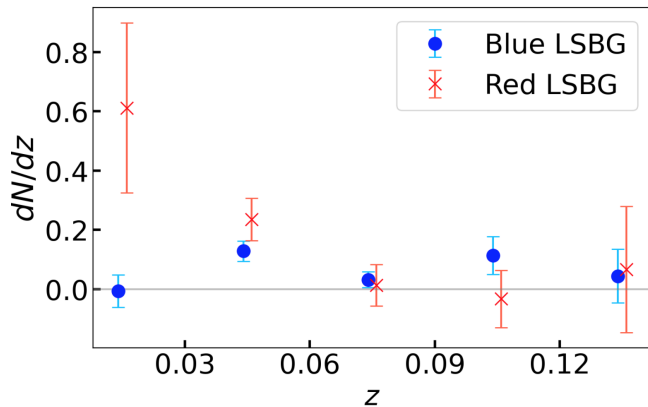


FIG. 2. The measured dN/dz amplitudes for red (cross markers) and blue (circles) LSBGs with $1\text{-}\sigma$ errorbars, obtained by cross-correlation with the 6dF galaxy sample.

We note that for the dN/dz measurement, we have used only LSBG and spec- z samples in the DES Y1 footprint ($\sim 1800 \text{ deg}^2$) because the random sample of the spec- z sample publicly, used in the angular cross-correlation measurement, is limited to samples within the footprint.

B. γ -ray flux modeling for DM annihilation

We model the γ -ray flux for the DM annihilation in target objects,

$$\frac{d\Phi_{\text{ann}}}{dE} = J \times \frac{\langle\sigma v\rangle}{8\pi m_\chi^2} \sum_i \text{Br}_i \frac{dN_i}{dE}, \quad (4)$$

where $\langle\sigma v\rangle$, m_χ , N_i and Br_i are the DM annihilation cross-section, DM mass, γ -ray photon flux and branching ratio of the i -th annihilation channel, respectively. In this work, we consider a representative channel, $b\bar{b}$. J is called as J-factor and defined,

$$J = [1 + b_{\text{sh}}(M_{\text{halo}})] \int_s ds' \int_\Omega d\Omega' \rho_{\text{DM}}^2(s', \Omega'), \quad (5)$$

where ρ_{DM} , s' and Ω denote the DM density, line-of-sight vector and angular size of target objects, respectively. We assume the NFW profile as the smoothed DM density profile. In addition to the smooth component, the annihilation signal is enhanced by the clumpy subhalo structure which is expressed with the boost factor, b_{st} . We set b_{st} to unity given the typical halo mass of the LSBG $\sim 10^{10} M_\odot$ [43]. Because of angular size of DES-LSBGs much smaller than the LAT PSF, we regard the objects as point-like sources, and then J-factor is simply written by the halo mass, the concentration parameter and angular diameter distance. To estimate the halo mass, we first convert the g , i and r band magnitude into the V band magnitude using $V = g - 0.59(g - r) - 0.01$ [44]. Given the

luminosity distance d_L by random assignment of object redshifts from the posterior distribution, we obtain the absolute magnitude M_V from $M_V = V + 5 - 5 \log_{10} d_L$, and then assuming the mass-to-light ratio to unity [45], we finally derive the halo mass from the stellar to halo mass relation [46]. For the concentration parameter, we apply the model [47]. For statistical uncertainties of the halo mass and density profile at $1\text{-}\sigma$ Gaussian error, we evaluate $\Delta \log M_{\text{halo}} = 0.4$ for scatter of the stellar-to-halo mass conversion [15] and $\Delta \log c = 0.1$ [48].

C. Composite likelihood

For the flux likelihood of our LSBG, we adopt the Bayesian method as described in section III B and define the likelihood of the annihilation γ -ray flux model for each LSBG as $\mathcal{L}(\alpha_{ij}|\langle\sigma v\rangle, J_i)$, where J_i and α_{ij} are the J-factor of i -th LSBG and the UGRB amplitude parameter at the object position in the j -th energy bin in Section III B, respectively. Given the density of LSBG sample in the sky, we assume that the flux amplitudes of all LSBGs are statistically independent of each other [21]. Then, the composite likelihood is given by $\log \mathcal{L}(\alpha|\langle\sigma v\rangle, J) = \sum_{ij} \log \mathcal{L}(\alpha_{ij}|\langle\sigma v\rangle, J_i)$. Here, we define a delta-likelihood, $\Delta \log \mathcal{L}(\alpha|\langle\sigma v\rangle, J) \equiv \log \mathcal{L}(\alpha|\langle\sigma v\rangle, J) - \log \mathcal{L}_0$, where \mathcal{L}_0 is the likelihood for zero flux of the annihilation γ -ray flux. Because of our LSBG flux models to be positive definite, $\Delta \log \mathcal{L}(\alpha|\langle\sigma v\rangle, J)$ are well-described the $\chi^2/2$ distribution with one degree of freedom via the Wilks theorem [37]. Therefore, the upper limit with 95% C.L. on the annihilation cross-section is given when $\Delta \log \mathcal{L}(\alpha|\langle\sigma v\rangle, J)$ decreases to $3.8/2$. To evaluate the total uncertainty for the upper-limit estimate, which comes from the dN/dz measurement error and uncertainties for the halo-property estimate, we iterate the Monte-Carlo resampling in 1000 times in terms of the modeling process of the annihilation γ -ray flux. For the dN/dz measurement error, we iterate random draw processes for individual object redshifts by using different dN/dz distributions whose amplitudes follow the posterior distribution described in IV A. For uncertainties of the halo mass and concentration, we give scatters of those Gaussian errors described in section IV B.

V. RESULT

In Figure 3, we provide upper limits on the annihilation cross-section at the $b\bar{b}$ channel in the black, red and blue solid lines, by the composite likelihood analysis of the annihilation γ -ray flux models for full, red and blue DES-LSBG samples, respectively. We show the total uncertainty for the upper limit with the full sample in the green shaded region of 95% containment in 1000 Monte-Carlo simulations. Although the number of the blue LSBGs are two times larger than that of the red LSBGs, the upper limits with both populations are simi-

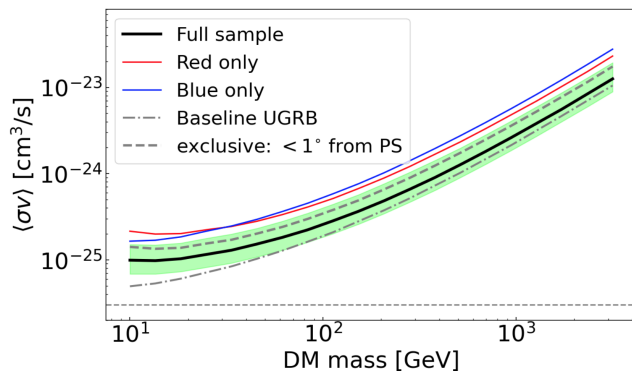


FIG. 3. The upper limits on the velocity-averaged DM annihilation cross-section at the $b\bar{b}$ channel as a function of DM masses. The black, red and blue solid lines are median values of the upper limits on the cross section from the full, red and blue samples of DES LSBGs, respectively. Green shaded region represents a 95% uncertainty region around the full sample constraint due to the random draw of the redshift. Thick dashed line show the constraint from the conservative sample (see text for detail). In the dash-dotted line, we show the constraint with all objects and the UGRB without the recalibration process described in Subsection III B. The horizontal line represents the prediction of the thermal relic cross section (3×10^{-26} [cm³/s]).

lar to each other, reflecting the fact that the blue LSBGs are distributed widely across all redshift ranges but red LSBGs are localized at lower redshifts.

For conservative constraints, we consider the sample removing neighboring objects with separation less than 1° from bright point sources because UGRB flux around the bright sources may be underestimated due to over-subtracting the model fluxes of the sources, which leads to provide a spuriously strong constraint. In Figure 3, we show the constraint from this conservative sample of 16,353 objects as dashed line. We find that the number of samples due to this selection decreases to $\sim 70\%$ and the constraint becomes $\sim 30\%$ weaker compared to the full sample. This implies that the constraint simply scales with the number of sample, which suggests that the use of the objects near the bright point sources do not induce spurious constraints in our analysis.

The dash-dotted line in Figure 3 represents the upper limit using the full LSBG sample and UGRB field with the recalibration process in Section III B. In all DM mass ranges, upper limits with the UGRB from recalibrated model parameters are weaker than those with the UGRB with no recalibration. As the photon statistics get large in lower energy, inaccurate parameter estimation affects to the likelihood analysis in lower energy and as a result, the upper limits in lower DM mass regimes have relative large variability.

VI. SUMMARY

In this work, we place the constraint on the DM annihilation cross-section by cross-correlating the DES-LSBG (23,790 objects in the sky coverage of $\sim 5,000$ deg²) without individual distance information to the UGRB photon field obtained by the *Fermi*-LAT observation in the energy range of 500 MeV to 500 GeV, accumulated over 12 years. As performed in our previous work [21], the distance of individual galaxy is randomly drawn from the estimated dN/dz distribution, which is measured by the cross-correlation of LSBGs with galaxies whose distances are spectroscopically identified. For the dN/dz measurement, we have estimated the angular cross-correlation of all red or blue LSBG samples with different redshift samples of the 6dFGS spec- z sample which is divided into five redshift bins with equal width in the range of $0 < z < 0.15$. We have computed the annihilation γ -ray flux for each LSBG by randomly drawing the redshift from the measured dN/dz distribution.

To obtain the putative flux of each LSBG, we have constructed the UGRB field in our ROIs with the LAT data and all γ -ray emission models for the diffuse and resolved sources taken from the 4FGL-DR2 source catalog and 79 newly detected sources with $TS \geq 25$ in our analysis, which is $\sim 11\%$ of the number of all resolved sources in our ROIs. After optimizing all model parameters of these sources in each ROI, we have performed the recalibration for model parameters of the diffuse and resolved sources around LSBGs, because the putative γ -ray flux, which is typically faint can be highly sensitive to the model parameters of bright sources [8]. The putative flux for the LSBG assuming the power-law flux model found to be significantly small because the TS values for most of the LSBGs are less than unity in most of the energy bins.

We have obtained the upper limit of the dark matter cross section of $\langle\sigma v\rangle < 3 \times 10^{-25}$ (95% C.L.) at $m_\chi = 100$ GeV from the composite likelihood for all DES-LSBGs using the recalibrated UGRB flux. To be conservative, we have removed LSBGs within 1° radius from resolved sources ($\sim 30\%$ of the total sample) because UGRB fluxes can be underestimated by the contamination from the bright sources, which may lead to a spuriously strong constraint. However, the amount of the degradation of constraint with this conservative sample selection is consistent with the expectation from the scaling of the number of objects, which indicates that the use of the LSBGs near the bright sources does not induce an unreasonably strong constraint. Furthermore, we have considered the impact of the recalibration of the bright-source model parameters on the DM constraint. We found that the upper limit using the UGRB flux with the recalibration is at most 2 times larger than the one using nonrecalibrated flux. Therefore, we conclude that the recalibration of the UGRB fluxes around bright sources is essentially important for this sort of analysis where the estimation of the faint γ -ray flux is important.

ACKNOWLEDGMENTS

We thank Oscar Macias for giving lots of kind supports, particularly for the use of the Fermi Science Tool,

and productive discussion. This work was supported in part by World Premier International Research Center Initiative, MEXT, Japan, and JSPS KAKENHI Grant No. 19H00677, 20H05850, 20H05855, 20J11682 and 21H05454.

-
- [1] G. Jungman, M. Kamionkowski, and K. Griest. Super-symmetric dark matter. *Physics Report*, 267:195–373, Mar 1996.
- [2] Giorgio Arcadi, Maíra Dutra, Pradipta Ghosh, Manfred Lindner, Yann Mambrini, Mathias Pierre, Stefano Profumo, and Farinaldo S. Queiroz. The waning of the WIMP? A review of models, searches, and constraints. *European Physical Journal C*, 78(3):203, March 2018.
- [3] Tongyan Lin. TASI lectures on dark matter models and direct detection. *arXiv e-prints*, page arXiv:1904.07915, Apr 2019.
- [4] Gianfranco Bertone, Dan Hooper, and Joseph Silk. Particle dark matter: evidence, candidates and constraints. *Physics Report*, 405(5-6):279–390, Jan 2005.
- [5] Leszek Roszkowski, Enrico Maria Sessolo, and Sebastian Trojanowski. WIMP dark matter candidates and searches—current status and future prospects. *Reports on Progress in Physics*, 81(6):066201, Jun 2018.
- [6] Oscar Macias and Chris Gordon. Contribution of cosmic rays interacting with molecular clouds to the Galactic Center gamma-ray excess. *Phys. Rev. D*, 89(6):063515, March 2014.
- [7] Shin’ichiro Ando, Aurélien Benoit-Lévy, and Eiichiro Komatsu. Mapping dark matter in the gamma-ray sky with galaxy catalogs. *Phys. Rev. D*, 90(2):023514, Jul 2014.
- [8] Ackermann, M. *et al.* Search for Extended Gamma-Ray Emission from the Virgo Galaxy Cluster with FERMI-LAT. *Astrophys. J.*, 812(2):159, October 2015.
- [9] T. Daylan, D. P. Finkbeiner, D. Hooper, T. Linden, S. K. N. Portillo, N. L. Rodd, and T. R. Slatyer. The characterization of the gamma-ray signal from the central Milky Way: A case for annihilating dark matter. *Physics of the Dark Universe*, 12:1–23, June 2016.
- [10] Ackermann, M. *et al.* The Fermi Galactic Center GeV Excess and Implications for Dark Matter. *Astrophys. J.*, 840(1):43, May 2017.
- [11] Kevork N. Abazajian, Shunsaku Horiuchi, Manoj Kaplinghat, Ryan E. Keeley, and Oscar Macias. Strong constraints on thermal relic dark matter from Fermi-LAT observations of the Galactic Center. *Phys. Rev. D*, 102(4):043012, August 2020.
- [12] R. Adam, H. Goksu, S. Brown, L. Rudnick, and C. Ferrari. γ -ray detection toward the Coma cluster with Fermi-LAT: Implications for the cosmic ray content in the hadronic scenario. *A&Ap.*, 648:A60, April 2021.
- [13] Charles Thorpe-Morgan, Denys Malyshev, Christoph-Alexander Stegen, Andrea Santangelo, and Josef Jochum. Annihilating dark matter search with 12 yr of Fermi LAT data in nearby galaxy clusters. *MNRAS*, 502(3):4039–4047, April 2021.
- [14] Sebastian Hoof, Alex Geringer-Sameth, and Roberto Trotta. A global analysis of dark matter signals from 27 dwarf spheroidal galaxies using 11 years of Fermi-LAT observations. *JCAP*, 2020(2):012, February 2020.
- [15] Daiki Hashimoto, Oscar Macias, Atsushi J. Nishizawa, Kohei Hayashi, Masahiro Takada, Masato Shirasaki, and Shin’ichiro Ando. Constraining dark matter annihilation with HSC low surface brightness galaxies. *JCAP*, 2020(1):059, January 2020.
- [16] Pooja Bhattacharjee, Pratik Majumdar, Mousumi Das, Subinoy Das, Partha S. Joarder, and Sayan Biswas. Multiwavelength analysis of low surface brightness galaxies to study possible dark matter signature. *MNRAS*, 501(3):4238–4254, March 2021.
- [17] Prole, D. J. *et al.* Halo mass estimates from the globular cluster populations of 175 low surface brightness galaxies in the Fornax cluster. *MNRAS*, 484(4):4865–4880, Apr 2019.
- [18] Wittmann, Carolin *et al.* A population of faint low surface brightness galaxies in the Perseus cluster core. *MNRAS*, 470(2):1512–1525, Sep 2017.
- [19] Wei Du, Cheng Cheng, Hong Wu, Ming Zhu, and Yougang Wang. Low Surface Brightness Galaxy catalogue selected from the α .40-SDSS DR7 Survey and Tully-Fisher relation. *MNRAS*, 483(2):1754–1795, Feb 2019.
- [20] Greco, J. P. *et al.* Illuminating Low Surface Brightness Galaxies with the Hyper Suprime-Cam Survey. *Astrophys. J.*, 857:104, April 2018.
- [21] Daiki Hashimoto, Atsushi J. Nishizawa, Masahiro Takada, and Oscar Macias. Dark matter constraint with gamma-ray galaxies cross correlation scales with N. *arXiv e-prints*, page arXiv:2109.08832, September 2021.
- [22] Tanoglidis, D. *et al.* (DES Collaboration). Shadows in the Dark: Low-surface-brightness Galaxies Discovered in the Dark Energy Survey. *ApJS*, 252(2):18, February 2021.
- [23] Flaugher, B. *et al.* The Dark Energy Camera. *AJ*, 150(5):150, November 2015.
- [24] Morganson, E. *et al.* The Dark Energy Survey Image Processing Pipeline. *PASP*, 130(989):074501, July 2018.
- [25] E. Bertin and S. Arnouts. SExtractor: Software for source extraction. *A&AS.*, 117:393–404, June 1996.
- [26] Sevilla-Noarbe, I. *et al.* Dark Energy Survey Year 3 Results: Photometric Data Set for Cosmology. *ApJS*, 254(2):24, June 2021.
- [27] Paola Marigo, Léo Girardi, Alessandro Bressan, Philip Rosenfield, Bernhard Aringer, Yang Chen, Marco Dussin, Ambra Nanni, Giada Pastorelli, Thaíse S. Rodrigues, Michele Trabucchi, Sara Bladh, Julianne Dalcanton, Martin A. T. Groenewegen, Josefina Montalbán, and Peter R. Wood. A New Generation of PARSEC-COLIBRI Stellar Isochrones Including the TP-AGB Phase. *Astrophys. J.*, 835(1):77, January 2017.
- [28] Jones, D. Heath *et al.* The 6dF Galaxy Survey: samples, observational techniques and the first data release. *MNRAS*, 355(3):747–763, December 2004.
- [29] D. Heath Jones, Mike A. Read, Will Saunders, Matthew Colless, Tom Jarrett, Quentin A. Parker, Anthony P.

- Fairall, Thomas Mauch, Elaine M. Sadler, Fred G. Watson, Donna Burton, Lachlan A. Campbell, Paul Cass, Scott M. Croom, John Dawe, Kristin Fiegert, Leela Frankcombe, Malcolm Hartley, John Huchra, Dionne James, Emma Kirby, Ofer Lahav, John Lucey, Gary A. Mamon, Lesa Moore, Bruce A. Peterson, Sayuri Prior, Dominique Proust, Ken Russell, Vicky Safouris, Ken-ichi Wakamatsu, Eduard Westra, and Mary Williams. The 6dF Galaxy Survey: final redshift release (DR3) and southern large-scale structures. *MNRAS*, 399(2):683–698, October 2009.
- [30] A. Drlica-Wagner, I. Sevilla-Noarbe, E. S. Rykoff, R. A. Gruendl, B. Yanny, D. L. Tucker, B. Hoyle, A. Carnero Rosell, G. M. Bernstein, K. Bechtol, M. R. Becker, A. Benoit-Lévy, E. Bertin, M. Carrasco Kind, C. Davis, J. de Vicente, H. T. Diehl, D. Gruen, W. G. Hartley, B. Leistedt, T. S. Li, J. L. Marshall, E. Neilsen, M. M. Rau, E. Sheldon, J. Smith, M. A. Troxel, S. Wyatt, Y. Zhang, T. M. C. Abbott, F. B. Abdalla, S. Alam, M. Banerji, D. Brooks, E. Buckley-Geer, D. L. Burke, D. Capozzi, J. Carretero, C. E. Cunha, C. B. D’Andrea, L. N. da Costa, D. L. DePoy, S. Desai, J. P. Dietrich, P. Doel, A. E. Evrard, A. Fausti Neto, B. Flaugher, P. Fosalba, J. Frieman, J. García-Bellido, D. W. Gerdes, T. Giannantonio, J. Gschwend, G. Gutierrez, K. Honscheid, D. J. James, T. Jeltema, K. Kuehn, S. Kuhlmann, N. Kuropatkin, O. Lahav, M. Lima, H. Lin, M. A. G. Maia, P. Martini, R. G. McMahon, P. Melchior, F. Menanteau, R. Miquel, R. C. Nichol, R. L. C. Ogando, A. A. Plazas, A. K. Romer, A. Roodman, E. Sanchez, V. Scarpine, R. Schindler, M. Schubnell, M. Smith, R. C. Smith, M. Soares-Santos, F. Sobreira, E. Suchyta, G. Tarle, V. Vikram, A. R. Walker, R. H. Wechsler, J. Zuntz, and DES Collaboration. Dark Energy Survey Year 1 Results: The Photometric Data Set for Cosmology. *ApJS*, 235(2):33, April 2018.
- [31] Feng-Jie Lei, Hong Wu, Yi-Nan Zhu, Wei Du, Min He, Jun-Jie Jin, Pin-Song Zhao, and Bing-Qing Zhang. An $H\alpha$ Imaging Survey of the Low Surface Brightness Galaxies Selected from the Spring Sky Region of the 40% ALFALFA H I Survey. *ApJS*, 242(1):11, May 2019.
- [32] Atwood, W. *et al.* Pass 8: Toward the Full Realization of the Fermi-LAT Scientific Potential. *arXiv e-prints*, page arXiv:1303.3514, March 2013.
- [33] M. Wood, R. Caputo, E. Charles, M. Di Mauro, J. Magill, J. S. Perkins, and Fermi-LAT Collaboration. Fermipy: An open-source Python package for analysis of Fermi-LAT Data. *International Cosmic Ray Conference*, 301:824, Jan 2017.
- [34] Fermi Science Support Development Team. Fermitools: Fermi Science Tools, May 2019.
- [35] The Fermi-LAT collaboration. Fermi Large Area Telescope Fourth Source Catalog. *arXiv e-prints*, page arXiv:1902.10045, Feb 2019.
- [36] J. Ballet, T. H. Burnett, S. W. Digel, and B. Lott. Fermi Large Area Telescope Fourth Source Catalog Data Release 2. *arXiv e-prints*, page arXiv:2005.11208, May 2020.
- [37] S. S. Wilks. The large-sample distribution of the likelihood ratio for testing composite hypotheses. *The Annals of Mathematical Statistics*, 9(1):60–62, 1938.
- [38] Mattox, J. R. *et al.* The Likelihood Analysis of EGRET Data. *Astrophys. J.*, 461:396, April 1996.
- [39] Nolan, P. L. *et al.* Fermi Large Area Telescope Second Source Catalog. *ApJS*, 199(2):31, Apr 2012.
- [40] S. D. Landy and A. S. Szalay. Bias and variance of angular correlation functions. *Astrophys. J.*, 412:64–71, July 1993.
- [41] Mike Jarvis. TreeCorr: Two-point correlation functions, August 2015.
- [42] Brice Ménard, Ryan Scranton, Samuel Schmidt, Chris Morrison, Donghui Jeong, Tamas Budavari, and Mubdi Rahman. Clustering-based redshift estimation: method and application to data. *arXiv e-prints*, page arXiv:1303.4722, March 2013.
- [43] N. Hiroshima, S. Ando, and T. Ishiyama. Modeling evolution of dark matter substructure and annihilation boost. *Phys. Rev. D*, 97(12):123002, June 2018.
- [44] Jester, S. *et al.* The Sloan Digital Sky Survey View of the Palomar-Green Bright Quasar Survey. *AJ*, 130:873–895, September 2005.
- [45] J. Woo, S. Courteau, and A. Dekel. Scaling relations and the fundamental line of the local group dwarf galaxies. *MNRAS*, 390:1453–1469, November 2008.
- [46] B. P. Moster, T. Naab, and S. D. M. White. Galactic star formation and accretion histories from matching galaxies to dark matter haloes. *MNRAS*, 428:3121–3138, February 2013.
- [47] Benedikt Diemer and Michael Joyce. An Accurate Physical Model for Halo Concentrations. *Astrophys. J.*, 871(2):168, February 2019.
- [48] A. A. Dutton and A. V. Macciò. Cold dark matter haloes in the Planck era: evolution of structural parameters for Einasto and NFW profiles. *MNRAS*, 441:3359–3374, July 2014.